The 9th European Congress on Computational Methods in Applied Sciences and Engineering
ECCOMAS Congress 2024
3–7 June 2024, Lisboa, Portugal

A BEAM MODEL FOR THE ELASTO-PLASTIC ANALYSIS OF METAL STRUCTURES CONSIDERING NORMAL STRESS-SHEAR STRESSES INTERACTION AND WARPING

DOMENICO MAGISANO[1] AND GIOVANNI GARCEA[1]

[1] Department of Computer Science, Modeling, Electronics and Systems Engineering,
University of Calabria,
87030 Rende (Cosenza), Italy
e-mail: domenico.magisano@unical.it, giovanni.garcea@unical.it

Key words: 3D frames, inelastic analysis, normal-shear stress, warping, mixed finite elements.

Summary. The fiber model evaluates the normal stress at a number of points over the section following the plane section assumption and, by integration, axial force and bending moments. The interaction with tangential stresses is neglected due to the inaccurate tangential strains of the kinematics. This work presents a generalized fiber model capable of considering interactions among all stress components. A preliminary cross-section analysis, based on the Saint Venant problem, provides the 3D strain as a function of the section generalized strains. This field, accurate also in the inelastic case, is exploited to impose at each section point a 3D von Mises elasto-plastic law, obtaining by integration all the resultants and moments with a full interaction. Non-uniform warping is also easily included. The section model is implemented in a mixed 3D beam-column finite element with equilibrated stress field, accurate with a minimal mesh. Numerical tests show the excellent prediction of the proposal compared to analytical and solid FEM solutions also for structures not flexure-dominated. Its efficiency, on the same order as a standard fiber model, makes the approach suitable also for large buildings.

1 INTRODUCTION

Fiber beam-column elements, as described by [1], offer a balanced blend of accuracy and efficiency in modeling structural members under axial force and biaxial bending. They use the assumption of the section remaining planar after deformation to relate generalized strains, i.e. axial strain and curvatures, to the distribution of normal strain across the section. This relationship allows for the evaluation of normal stress at integration points (fibers) across the section, enabling numerical integration to determine axial force and bending moments. Apart from conventional incremental analyses, the fiber model finds application in evaluating fire resistance [2] and shakedown analysis [3].

The main limitation of this model lies in its incapacity to consider tangential stress components arising from shear forces and torsion at the point level. The reason is that, when computed directly from the kinematics based on the rigid section deformation, the shear strains can be largely inaccurate for typical sections. There has long been a need for a refined element capable of automatically modeling member responses under high shear and torsion, interacting with axial force and bending moments.

Many research activities have been spent in the attempt of an accurate modeling of this interaction. Petrangeli et al.[4] initiated research on inelastic shear behavior in reinforced concrete elements, considering its interaction with axial force and bending moment. Marini et al. [5] proposed fiber beam elements with simplified constitutive laws for shear. Saritas [6] presented a formulation for seismic assessment of steel structures, while Navarro et al. [7] focused on reinforced and prestressed concrete elements. Papachristidis et al. [8] addressed steel frames, while works by Gruttmann et al. [9] and Battini [10] considered torsional warping. Bleyer [11] discussed shell-like elastoplasticity.

Mixed finite element formulations [12, 13] are widely used for inelastic analysis of frames yielding accurate results with fewer global degrees of freedom with respect to displacement formulations. Furthermore stress degrees of freedom are local on the element and can be condensed before solving global linear systems, reducing the computational burden. Material laws are applied at predefined control sections, typically Gauss-Lobatto points. Compared to displacement-based elements, mixed elements require solving a small system of equations at the element level (element state determination) to ensure consistency with the constitutive law. Equations are derived from the Hu-Washizu weak form of the problem [12], solved with global structural equilibrium. Alternatively, element state can be solved at each global Newton iteration [14, 15].

A generalized fiber model for steel frames is presented here that automatically considers interactions among all stress components. It utilizes a preliminary finite element cross-section analysis based on the generalized De Saint Venant (SV) elastic problem [16, 17] to establish accurate 3D elastic strains across the section. This analysis, performed once, remains accurate even in the inelastic case. The resulting strain field is then used to assess 3D stress at each section point via a von Mises associated plasticity law, allowing integration of all resultants and moments with full interaction. This refined approach improves accuracy and reliability in the inelastic range, especially for structures not dominated by flexure.

The proposed cross-section model is implemented in a mixed beam finite element with equilibrated stress field, accurate with a minimal mesh. The element is based on the usual 6 kinematic degrees of freedom (DOFs) for each end-node. Non-uniform warping, such as the torsional one, can be also easily included, with just an additional variable per end-node. The additional warping unknown is, however, required only to model non-uniform warping, since the uniform case is already considered in the 6 DOFs formulation.

A campaign of numerical tests (see [17]) validates the proposal against more detailed simulations based of solid finite elements. The extension of the proposal to the finite deformation case is very easy [15].

2 THE 3D BEAM MODEL

The 3D beam model used is based on the generalized SV solution, which also incorporates variability in torsional warping along the beam axis and plasticity.

2.1 The beam model with variable warping from the 3D continuum

Let us consider the beam as a Cauchy body $\mathcal{B}$. In the reference configuration and adopting a fixed Cartesian frame with origin $\mathcal{O}$ and basis vectors $\mathbf{e}_1, \mathbf{e}_2, \mathbf{e}_3$, each point is defined by a position vector $\mathbf{X} = s\mathbf{e}_1 + \mathbf{x}$, where $s \equiv x_1$ represents a one-dimensional abscissa along the axis line of length ℓ, and $\mathbf{x} = x_2\mathbf{e}_2 + x_3\mathbf{e}_3$ lies on the cross-section fiber(s) (see Fig. 1).

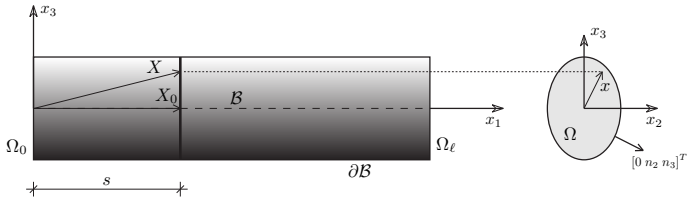

Figure 1: The cylindrical solid.

The displacement field $\mathbf{u}[\mathbf{X}]$ of the beam model is defined by the mean translation and rotation $\mathbf{v}(s)$ and $\boldsymbol{\varphi}(s)$ of the section plus an additional term accounting for variable warping effects

$$\mathbf{u}(\mathbf{X}) = \mathbf{v}(s) + \boldsymbol{\varphi}(s) \times \mathbf{x} + \mu(s)\boldsymbol{\omega}(\mathbf{x}), \tag{1}$$

where the operator $\times$ denotes the cross product, while $\boldsymbol{\omega}$ is the warping shape amplified by the $\mu(s)$. In this work, only torsional out-of-plane warping is considered and then

$$\boldsymbol{\omega}(\mathbf{x}) = \omega(\mathbf{x})\mathbf{e}_1. \tag{2}$$

Adopting a Voigt notation the non-zero strain components $\boldsymbol{\varepsilon} = [\varepsilon_{11}, \gamma_{12}, \gamma_{13}]^T$ can be written as

$$\boldsymbol{\varepsilon}(s, \mathbf{x}) = \boldsymbol{\eta}(s) + \mathbf{W}_x^T\boldsymbol{\chi}(s) + \mathbf{A}_\omega(\mathbf{x})\mu_{,s}\,(s) + \mathbf{D}_\omega(\mathbf{x})\mu(s) = \bar{\mathbf{B}}(\mathbf{x})\boldsymbol{\rho}(s) \tag{3}$$

where a comma denoting derivative and

$$\mathbf{W}_x = \mathrm{spin}(\mathbf{x}) = \begin{bmatrix} 0 & -x_3 & x_2 \\ x_3 & 0 & 0 \\ -x_2 & 0 & 0 \end{bmatrix} \qquad \mathbf{A}_\omega = \begin{bmatrix} \omega \\ 0 \\ 0 \end{bmatrix} \qquad \mathbf{D}_\omega = \begin{bmatrix} 0 \\ \omega_{,2} \\ \omega_{,3} \end{bmatrix},$$

the vector of generalized strains of the section is $\boldsymbol{\rho}(s) = \{\boldsymbol{\eta}, \boldsymbol{\chi}, \mu_{,s}\,, \mu\}$ and the overall compatibility operator $\bar{\mathbf{B}}$ are self-defined. Vector $\boldsymbol{\eta}$ collects the axial and shear strains, $\boldsymbol{\chi}$ the torsional and bending curvatures:

$$\boldsymbol{\eta}(s) \equiv \begin{bmatrix} e \\ \gamma_2 \\ \gamma_3 \end{bmatrix} = \begin{bmatrix} v_{1,s} \\ v_{2,s} - \varphi_3 \\ v_{3,s} + \varphi_2 \end{bmatrix} \qquad \boldsymbol{\chi}(s) \equiv \begin{bmatrix} \chi_1 \\ \chi_2 \\ \chi_3 \end{bmatrix} = \begin{bmatrix} \varphi_{1,s} \\ \varphi_{2,s} \\ \varphi_{3,s} \end{bmatrix}. \tag{4}$$

Letting $\boldsymbol{\sigma} = [\sigma_{11}, \sigma_{12}, \sigma_{13}]^T$ the vector of the active stress components, the kinematics assumed in Eq. (3) allows us to write the virtual internal work $\mathcal{W}$ as

$$\mathcal{W} := \int_\ell \int_\Omega \boldsymbol{\sigma}^T \boldsymbol{\varepsilon} dA ds = \int_\ell \left(\boldsymbol{\mathcal{N}}(s)^T\boldsymbol{\eta}(s) + \boldsymbol{\mathcal{M}}(s)^T\boldsymbol{\chi}(s) + \mathcal{B}\mu_{,s}\,(s) + \mathcal{T}\mu(s)\right) ds = \int_\ell \mathbf{t}(s)^T\boldsymbol{\rho}(s)\, ds \tag{5}$$

so defining the vector of the generalized internal actions for the beam $\mathbf{t}(s) = \{\boldsymbol{\mathcal{N}}, \boldsymbol{\mathcal{M}}, \mathcal{B}, \mathcal{T}\}$ which collects the classical stress resultants $\boldsymbol{\mathcal{N}}$ and moments $\boldsymbol{\mathcal{M}}$ on the section plus the new quantities $\mathcal{B}$, called bi-moment, and $\mathcal{T}$, known as bi-shear

$$\begin{bmatrix} \boldsymbol{\mathcal{N}} \\ \boldsymbol{\mathcal{M}} \\ \mathcal{B} \\ \mathcal{T} \end{bmatrix} = \begin{bmatrix} \int_\Omega \boldsymbol{\sigma} dA \\ \int_\Omega \mathbf{W}_x\boldsymbol{\sigma} dA \\ \int_\Omega \mathbf{A}_\omega^T\boldsymbol{\sigma} dA \\ \int_\Omega \mathbf{D}_\omega^T\boldsymbol{\sigma} dA \end{bmatrix} \qquad \text{and then} \qquad \mathbf{t}(s) = \int_\Omega \bar{\mathbf{B}}(\mathbf{x})^T\boldsymbol{\sigma} dA \tag{6}$$

The model is completed with a suitable constitutive law. In the linear elastic case we have

$$\mathbf{t}(s) = \mathbf{C}\boldsymbol{\rho}(s). \tag{7}$$

The constitutive matrix $\mathbf{C}$, when derived by the 3D continuum using the assumed kinematics, need to be corrected. In our proposal, this problem will be avoided by replacing the matrix $\bar{\mathbf{B}}$ in Eq. (3) with that coming from the generalized SV elastic solution [16, 17].

2.2 Saint Venant cross-section analysis

By exploiting a cross-section discretization into 2D elements and employing a semi-analytical solution, the cross-section analysis [16, 17] enables the consideration of the 3D strain field arising from the generalized SV solution, including variable torsional warping, by solving a series of linear problems on the discretized cross-section once and for all. The strain becomes

$$\boldsymbol{\varepsilon}_{3D}(\mathbf{x}, s) = \mathbf{L}_\epsilon(\mathbf{x})\mathbf{Q}_\alpha\boldsymbol{\alpha}(s) \quad \boldsymbol{\sigma}_{3D}(\mathbf{x}, s) = \mathbb{C}\boldsymbol{\varepsilon}_{3D}(\mathbf{x}, s) \tag{8}$$

where $\mathbf{L}_\epsilon(\mathbf{x})$ is the strain/displacement matrix, $\mathbf{Q}_\alpha$ is a modal matrix containing the cross section shapes in terms of cross section DOFs, $\boldsymbol{\alpha}(s)$ are the modes amplitude.

By exploiting the definition of the generalized stresses $\mathbf{t}$ we can express $\boldsymbol{\alpha}(s) = \mathbf{R}^{-1}\mathbf{t}(s)$ as a function of $\mathbf{t}(s)$ and then we have that

$$\boldsymbol{\sigma}_{3D}(\mathbf{x}, s) = \mathbf{N}_\sigma(\mathbf{x})\mathbf{t}(s) \quad \text{with} \quad \mathbf{N}_\sigma(\mathbf{x}) = \mathbb{C}\boldsymbol{\varepsilon}_{3D}\mathbf{L}_\epsilon(\mathbf{x})\mathbf{Q}_\alpha\mathbf{R}^{-1}. \tag{9}$$

The stationary of the strain energy in mixed Hellingher-Reissner form with respect to $\mathbf{t}$ furnishes the generalized elastic constitutive law of the section

$$\mathbf{t} = \mathbf{C}\boldsymbol{\rho} \quad \text{with} \quad \mathbf{C}^{-1} = \mathbf{F} = \int_\Omega \mathbf{N}_\sigma(\mathbf{x})^T\mathbb{C}_{3D}^{-1}\mathbf{N}_\sigma(\mathbf{x})d\Omega. \tag{10}$$

where the so define section constitutive matrix $\mathbf{C}$ automatically includes the effect of shear and uniform and non-uniform torsional warping with the correct stiffness constants and their coupling. The link between the section generalized strains $\boldsymbol{\rho}$ work-conjugate of $\mathbf{t}$ and the correct strain field over the section $\boldsymbol{\varepsilon}_{3D}$ coming from the generalized SV model can be obtained using the elastic constitutive law as

$$\boldsymbol{\varepsilon}_{3D}(\mathbf{x}, s) = \mathbf{B}_{3D}(\mathbf{x})\boldsymbol{\rho}(s). \tag{11}$$

The Timoshenko beam model of Section 2.1 can be made energetically equivalent, in the elastic case, to the SV model by using Eq. (11) to link the correct 3D strain field in the section with the generalized strains of the beam instead of Eq. (3).

2.3 Inelastic case

The SV strain approximation, Eq. (11), remains accurate even in the plasticity range, crucial for generalizing the section's fiber model. This enables us to apply a 3D elasto-plastic constitutive law at each section integration point, ensuring full stress component coupling. For typical metal members with isotropic thin-walled sections we have that $\sigma_{22} = \sigma_{33} = \sigma_{22} = 0$ and the Poisson coupling among the normal strain components has a negligible influence. This can be exploited to write the constitutive law directly in terms of the active stress $\boldsymbol{\sigma} = [\sigma_{11}, \sigma_{12}, \sigma_{13}]^T$ and strain

$\boldsymbol{\varepsilon} = [\varepsilon_{11}, \gamma_{12}, \gamma_{13}]^T$ components only allowing a computationally efficient stress evaluation at each point of the section by solving a closest point projection problem with only 3 stress unknowns. The incremental elasto-plastic equations for each control point m of the section discretization, integrated by a Backward Euler scheme, are

$$\begin{cases} \Delta\boldsymbol{\sigma}_m - \mathbb{C}\left(\Delta\boldsymbol{\varepsilon}_m - \Delta\mu_m \left.\dfrac{\partial f(\boldsymbol{\sigma})}{\partial\boldsymbol{\sigma}}\right|_{\boldsymbol{\sigma}=\boldsymbol{\sigma}_m}\right) = 0 \\ \Delta\mu_m \geq 0 \quad \Delta\mu_m f(\boldsymbol{\sigma}_m) = 0 \end{cases} \tag{12}$$

where $\mathbb{C} = \text{diag}\left\{E, G, G\right\}$, μ is the plastic multiplier, $f(\boldsymbol{\sigma})$ is the von Mises yield function

$$f(\boldsymbol{\sigma}) = \sigma_{11}^2 + 3(\sigma_{12}^2 + \sigma_{13}^2) - \sigma_y^2 \leq 0 \tag{13}$$

and the symbol Δ denotes the difference of the current variables and those consolidated at the end of the previous time step. The increment of active strains is computed as

$$\Delta\boldsymbol{\varepsilon}(\mathbf{x}, s) = \mathbf{B}(\mathbf{x})\Delta\boldsymbol{\rho}(s) \tag{14}$$

where $\mathbf{B}$ is a block of $\mathbf{B}_{3D}$ stored at each integration point of the section after the preliminary cross-section analysis. Perfect plasticity is considered here for simplicity.

3 THE MIXED FINITE ELEMENT FOR THE INELASTIC ANALYSIS

An equilibrated mixed finite element, allowing to obtain accurate results with few elements per member is adopted. The element uses exact shape functions for stress resultants and moments [2, 3] and an equilibrated interpolation for bi-moment and bi-shear. Kinematic variables are required only at the end nodes of the element. The kinematic degrees of freedom (DOFs) are 7 per node, i.e. the standard 6 of the Timoshenko beam plus the non-uniform warping amplitude. The model with 6 DOFs is obtained by eliminating warping from the kinematics [17].

3.1 The mixed finite element

The beam finite element is based on a stress approximation

$$\mathbf{t}(s) = \mathbf{D}(s)\boldsymbol{\beta}_e \tag{15}$$

which exactly satisfies the equilibrium equations on the element for zero body forces, i.e.

$$\boldsymbol{\mathcal{N}}_{,s} = \mathbf{0}, \qquad \boldsymbol{\mathcal{M}}_{,s} + \mathbf{e}_1 \wedge \boldsymbol{\mathcal{N}} = \mathbf{0}, \qquad \mathcal{B}_{,s} = \mathcal{T}. \tag{16}$$

Body load effects are exactly included as a particular solution of such differential equations. Equation (16) states that the resultants $\boldsymbol{\mathcal{N}} \equiv [N_1, N_2, N_3]^T$ and the torsional moment M_1 are constant, while the two bending components $M_2(s)$ and $M_3(s)$ of $\boldsymbol{\mathcal{M}}(s) \equiv [M_1, M_2, M_3]^T$ are linear with s and linked to the shear resultants so that $N_2\ell = -(M_3(\ell) - M_3(0))$ and $N_3\ell = (M_2(\ell) - M_2(0))$. A cubic polynomial interpolation is adopted for the bi-moment.

The internal work in Eq. (5) becomes

$$\mathcal{W} \equiv \boldsymbol{\mathcal{N}}^T(\mathbf{v}(\ell) - \mathbf{v}(0)) + \boldsymbol{\mathcal{M}}(\ell)^T\boldsymbol{\varphi}(\ell) - \boldsymbol{\mathcal{M}}(0)^T\boldsymbol{\varphi}(0) + \mathcal{B}(\ell)\mu(\ell) - \mathcal{B}(0)\mu(0) = \boldsymbol{\beta}_e^T\mathbf{Q}_e\mathbf{d}_e \tag{17}$$

allowing us to obtain directly the discrete form of $\mathcal{W}$ without any FE interpolation for the kinematic fields $\mathbf{u}(s)$, $\boldsymbol{\varphi}(s)$ and $\mu(s)$. In Eq. (17), the vectors collecting the kinematic $\mathbf{d}_e$ and static $\boldsymbol{\beta}_e$ FE parameters and the compatibility operator $\mathbf{Q}_e$ are defined as

$$\boldsymbol{\beta}_e = \begin{bmatrix} N_1 \\ M_2(0) \\ M_3(0) \\ M_2(\ell) \\ M_3(\ell) \\ M_1 \\ \mathcal{B}(0) \\ \mathcal{B}(\ell/3) \\ \mathcal{B}(2\ell/3) \\ \mathcal{B}(\ell) \end{bmatrix}, \quad \mathbf{d}_e = \begin{bmatrix} \mathbf{v}(0) \\ \boldsymbol{\varphi}(0) \\ \mathbf{v}(\ell) \\ \boldsymbol{\varphi}(\ell) \\ \mu(0) \\ \mu(\ell) \end{bmatrix}, \quad \mathbf{Q}_e = \frac{1}{\ell} \begin{bmatrix} -\ell\,\mathbf{e}_1^T & \mathbf{0} & \ell\,\mathbf{e}_1^T & \mathbf{0} & 0 & 0 \\ \mathbf{e}_3^T & -\ell\,\mathbf{e}_2^T & -\mathbf{e}_3^T & \mathbf{0} & 0 & 0 \\ -\mathbf{e}_2^T & -\ell\,\mathbf{e}_3 & \mathbf{e}_2^T & \mathbf{0} & 0 & 0 \\ -\mathbf{e}_3^T & \mathbf{0} & \mathbf{e}_3^T & \ell\,\mathbf{e}_2^T & 0 & 0 \\ \mathbf{e}_2^T & \mathbf{0} & -\mathbf{e}_2^T & \ell\,\mathbf{e}_3^T & 0 & 0 \\ \mathbf{0} & -\ell\,\mathbf{e}_1^T & \mathbf{0} & \ell\,\mathbf{e}_1^T & 0 & 0 \\ \mathbf{0} & \mathbf{0} & \mathbf{0} & \mathbf{0} & -1 & 0 \\ \mathbf{0} & \mathbf{0} & \mathbf{0} & \mathbf{0} & 0 & 0 \\ \mathbf{0} & \mathbf{0} & \mathbf{0} & \mathbf{0} & 0 & 0 \\ \mathbf{0} & \mathbf{0} & \mathbf{0} & \mathbf{0} & 0 & 1 \end{bmatrix}. \tag{18}$$

The $\boldsymbol{\beta}_e$ are local to each element and can be condensed out before assembling the global (structural) equations in the kinematic DOFs only.

3.2 The incremental elasto-plastic analysis

The elasto-plastic solution, for an external load linearly increasing with a load multiplier λ is obtained, as usual, by means of an incremental step-by-step analysis.

3.2.1 The elasto-plastic step equations for an equilibrated beam element

The equations defining the final state at each elasto-plastic increment of a step-by-step process for mixed finite elements, can be derived [12, 15], from a Hu-Washizu weak form. For elasto-plasticity, an equivalent alternative derivation is given in [3, 2, 18]. Starting from an initial stress state $\boldsymbol{\sigma}_m^{(0)}$ stored at each integration point m of the generic section g corresponding to a Gauss-Lobatto point of the beam FE, the elasto-plastic solution for the whole FE model can be obtained by solving at each step the following 3 groups of equations:

$$\text{Global equations} \quad \mathbf{Q}^T\boldsymbol{\beta}(\lambda) - \lambda\mathbf{p} - \mathbf{p}_0 = \mathbf{0} \tag{19a}$$

$$\text{Element equations} \quad \begin{cases} \mathbf{Q}_e\Delta\mathbf{d}_e - \displaystyle\sum_g \mathbf{D}_g^T\Delta\boldsymbol{\rho}_g w_g = \mathbf{0} \\ \mathbf{t}_g(\boldsymbol{\sigma}_1, \cdots, \boldsymbol{\sigma}_N) - \mathbf{D}_g\boldsymbol{\beta}_e - \lambda\bar{\mathbf{t}}_g = \mathbf{0} \qquad \forall g \end{cases} \tag{19b}$$

$$\text{Section equations} \quad \begin{cases} \Delta\boldsymbol{\varepsilon}_m = \mathbf{B}_m\Delta\boldsymbol{\rho}_g \\ \begin{cases} \Delta\boldsymbol{\sigma}_m - \mathbb{C}\left(\Delta\boldsymbol{\varepsilon}_m - \Delta\mu_m \left.\dfrac{\partial f(\boldsymbol{\sigma})}{\partial\boldsymbol{\sigma}}\right|_{\boldsymbol{\sigma}=\boldsymbol{\sigma}_m}\right) = 0 \\ \Delta\mu_m \geq 0 \quad \mu_m f(\boldsymbol{\sigma}_m) = 0 \end{cases} \\ \mathbf{t}_g = \displaystyle\sum_m \mathbf{B}_m^T\boldsymbol{\sigma}_m w_m \end{cases} \tag{19c}$$

where the symbol Δ denotes the increment of a generic quantity over the step, while w represents the generic weight of the numerical integration over the section and along the beam axis.

The global equations impose the equilibrium at structural level of internal $\mathbf{Q}^T\boldsymbol{\beta}$ and external forces $\lambda\mathbf{p}+\mathbf{p}_0$ obtained by assembling the element counterpart. The element-wise equations link the stress DOFs $\boldsymbol{\beta}_e$ with the displacement increment $\Delta\mathbf{d}_e$ by preserving the kinematic compatibility of the generalized strain increment $\Delta\boldsymbol{\rho}_g$ at each Gauss-Lobatto integration point g along the beam axis with the element displacement increment $\Delta\mathbf{d}_e$ and the FE equilibrated stress interpolation in Eq. (15). Vector $\lambda\bar{\mathbf{t}}_g$ collects the generalized stresses at the gth IP corresponding to the particular solution of the equilibrium equations due to distributed loads amplified by λ. Finally, the section generalized stresses $\mathbf{t}_g$ are obtained by numerical integration of the active stresses $\boldsymbol{\sigma}$ over the section corresponding to the increment of generalized strains $\Delta\boldsymbol{\rho}$. For that purpose, the associated elastic-perfectly plastic equations, written in finite incremental form through the backward Euler scheme, are imposed at each integration point m of the section for an increment of active strains $\Delta\boldsymbol{\varepsilon}_m$ computed from $\Delta\boldsymbol{\rho}$ through the compatibility SV matrix $\mathbf{B}$.

3.3 Strain-driven solution scheme

Instead of solving Eqs. (19) all together, it is possible to apply a strain-driven decomposed strategy based on the solution of the following three nested sub-steps.

- A *section state determination* provides the cross section generalize stresses $\mathbf{t}_g$ at each Gauss-Lobatto IP g along the element axis as a function of an assigned section generalized strain increment $\Delta\boldsymbol{\rho}_g$ and the current load multiplier λ using the constitutive law (19c). This requires the solution of a closest point projection problem at each integration point of the section, with $\mathbf{t}_g$ obtained by numerical integration of the resulting stress.

- An *element state determination* finds the element stress interpolation variables $\boldsymbol{\beta}_e$ corresponding to an assigned increment of element nodal kinematic variables $\Delta\mathbf{d}_e$ and the current load multiplier λ by means of the element equations (19b). An iterative solution at FE level involving, at each iteration, the section state determination at the IPs is required.

- A *global incremental-iterative process*, corresponding to a modified Riks method, solves the global equilibrium equations (19a) step-by-step with the stress interpolation variables $\boldsymbol{\beta}$ expressed as functions of the unknown kinematic degrees of freedom $\mathbf{d}$ and the current load multiplier λ through the element state determination.

The process allows to write the global equations in a standard strain-driven format with an arc-length incremental method providing a path of equilibrium points $(\lambda^{(n)},\mathbf{d}^{(n)})$.

4 Numerical Tests

Some numerical tests are reported and the results compared with analytical or solid FE solutions obtained with the commercial software Abaqus. A more complete campaign of numerical tests can be found in [17]. The material used for all tests is steel characterized by a Young modulus $E=2100000$ daN/cm^2, Poisson coefficient $\nu=0.3$ and yield stress $\sigma_y=2000$ daN/cm^2. The cross-section shapes reported in Fig. 2 and Tab. 1 are considered.

Different cross-section models are considered and compared adopting the following notation.

- SV: the proposed method. Non-uniform torsional warping is excluded.

- SVW: the proposed method with non-uniform torsional warping.

Name	Section dimensions			
	B	H	e	s
HEA300	30	29	1.40	0.85
IPE330	16	33	1.15	0.75
BOX160	16	16	0.80	0.80

Table 1: Dimensions (cm) of the sections.

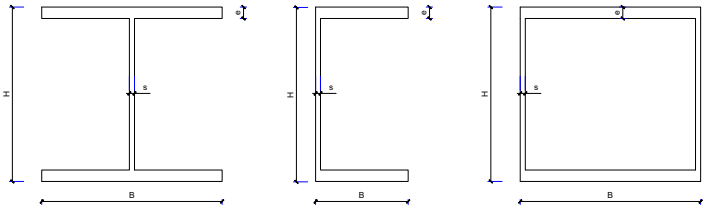

Figure 2: Shapes of the sections.

- SVW-free: SVW with torsional warping not restrained at the clamped sections.
- PS: the standard Timoshenko beam kinematics. Non-uniform torsional warping is excluded. This model was used in some previous works, e.g. [8].
- Abaqus: solid finite element solution provided by the commercial software Abaqus/Standard for a converged mesh.

In some tests, a comparison neglecting shear stresses, i.e. considering a simplified yield function $f(\sigma_{11}) = \sigma_{11}^2 - \sigma_y^2 \leq 0$ instead of the von Mises one is added. To denote such a case, -σ_{11} is added to the previously defined model names, e.g. SV-σ_{11}.

As expected, SV and SVW-free (free warping allowed to be uniform) provide identical solutions in the linear elastic case. Interestingly, the two models can differ in the plastic range, because the collapse mechanism obtained by SV satisfies compatibility and stress admissibility also for SVW-free, but not vice versa. SVW-free, with a richer kinematics, can find a different plastic mechanism associated to a lower collapse load, closer to the 3D continuum value for the given boundary condition. The equilibrium curves are reported in terms of load factor λ vs maximum displacement component in absolute value d_{max} in the whole structure.

4.1 Clamped-clamped beam subjected to uniform load

A clamped-clamped beam with HEA300 cross-section subjected to a uniform distributed transverse load $q = \lambda \cdot 1$ daN/cm along the strong axis of bending is considered. The presence of tangential stresses affects significantly the results, making it possible to compare the accuracy of the proposal with other methods. The results has been obtained using 2 elements for the beam with the cross-section discretized using $(6 \times 6) \times 1$ Q9 elements. No increase in accuracy is observed by using finer meshes for the section, while the beam finite element is exact in this case. The predictions of the SV model are compared with those of Abaqus using solid elements in Tab. 2, including also the results obtained using the Timoshenko-like plane section (PS) [8] and those given by the proposed SV-σ_{11}. In this last case, the results are coincident with the analytical value (for normal stresses only) calculated as

$$\lambda = \frac{16 M_y}{q \ell^2} \quad \text{with} \quad M_y = 2610137 \text{ daN·cm}$$

with the plastic bending moment M_y evaluated by assuming the section completely yielded with a symmetric distribution of positive and negative σ_{11}.

The prediction of the collapse multiplier is reported in Tab. 2 for the different models and beam lengths, allowing the following considerations: i) the SV model furnishes results close to

ℓ (cm)	λ			
	SV	Abaqus	SV-σ1	PS
300	248.46	240.25	464.02	432.75
350	211.67	200.30	340.92	324.11
400	182.34	170.76	261.01	251.25
500	137.15	132.95	167.05	163.14
600	104.20	104.98	116.00	114.16

Table 2: Clamped-clamped beam: collapse load multiplier for different beam lengths and models.

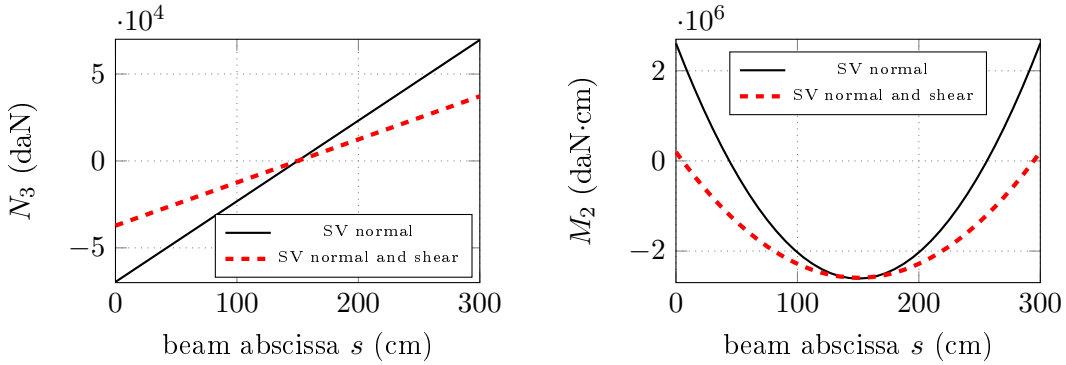

Figure 3: Clamped beam with $L = 300$ cm: shear force and bending moment at the collapse state.

the Abaqus solid solution also for short members where shear dominates the plastic behavior; ii) the PS model provides results very similar to SV-σ_{11} due to the inaccurate shear strain field; iii) SV-σ_{11} and PS largely overestimate the solid solution also for $\ell = 600$ cm, i.e. the shear-bending interaction is important also for length-to-height ratio up to 20. Moreover, for the shortest case of $\ell = 300$ cm (length-to-height ratio equal to 10) shear force and bending moment diagrams at incipient collapse are reported in Fig. 3 for SV and SV-σ_{11}. SV-σ_{11} gives the classical solution with M_y at 3 plastic hinges corresponding to end-sections and the mid-span leading to a huge error in the collapse load compared to the solid solution. Instead, SV is able correctly capture the shear plasticization at the clamped sections.

4.2 Simple 2D frame with shear links

A simple 2D frame (see Fig. 4) is considered. A horizontal force of $F = \lambda \cdot 1$ kN is applied at the top left node. A single element per member is employed. For beams and columns, IPE330 and HEA300 cross-sections are used respectively, with a $(6\times6)\times1$ discretization. A BOX section $160 \times 160 \times 8$ is used for the diagonals, subjected only to axial force, and then to a constant stress state over the section. 1 element per wall is used in this case.

In Fig. 5, the significant stress components at collapse for the central section of the IPE330 beam obtained by the SV model are reported. At this point, the only non-zero internal actions are normal and shear force. The normal stress is entirely distributed in the flanges, while yield limit for the shear stress $\sigma_y/\sqrt{3}$ is reached on the web.

The equilibrium path evaluated accounting for or neglecting the shear stresses are also presented in Fig. 6. The collapse load prediction is $\lambda = 5.424$ when tangential stresses are considered and $\lambda = 7.376$ when they are neglected. A total number of 18 step and 28 global iterations is

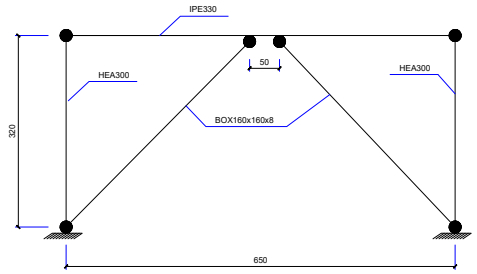

Figure 4: 2D frame with shear link

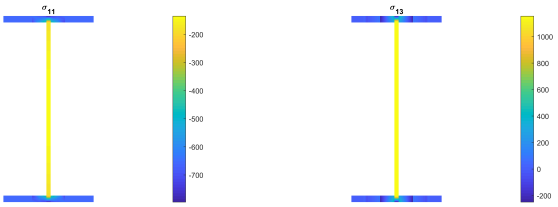

Figure 5: 2D frame: stress distribution at collapse at the middle section of the IPE330 shear link beam.

required by the incremental-iterative process. The computational cost is, in our `Matlab` implementation, of about 1 second.

5 CONCLUSIONS

The interaction of normal and tangential stresses is usually neglected or considered in a simplified way in the evaluation of the inelastic response of steel members. This work aimed at filling this gap in modeling with a very simple approach, easy to implement in commercial codes for practical applications. The proposal is based on the generalized SV solution, used to define, in a pre-processing stage, the link between the generalized strains of a beam model and the distribution of normal and tangential strains over the cross-section. Although this relationship is evaluated in the elastic case it still proves to be an excellent and robust approximation also in elasto-plastic analysis for typical metal sections. The effect of non-uniform torsional warping can be also easily included or excluded in the formulation. The proposed section model was implemented in a mixed finite element of beam, where the equilibrated solution of generalized stresses is adopted to achieve converged results with a minimal mesh and to express the kinematics in terms of DOFs at the end-nodes only, i.e. the only global variables. The approach provides very accurate and reliable predictions of the behavior of steel structures also when shear and torsion become important, compared to the solid reference solution.

REFERENCES

[1] E. Spacone, F. C. Filippou, F. F. Taucer, Fibre beam–column model for non–inear analysis of R/C frames: part I. Formulation, Earthquake Engineering and Structural Dynamics 25 (7) (1996) 711–725.

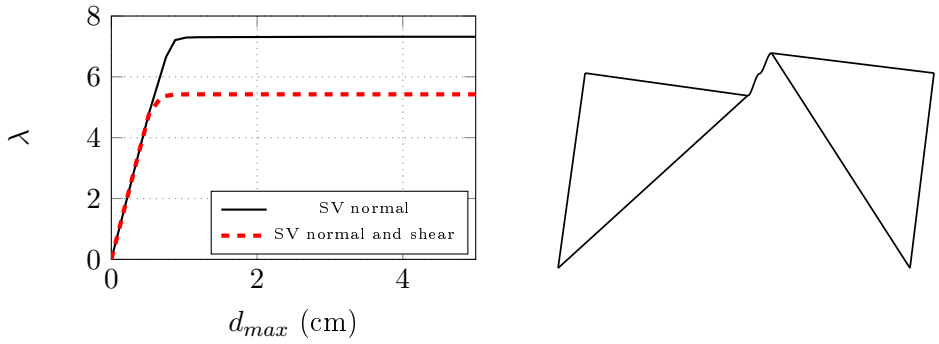

(a) Load amplifier vs displacement curve (b) Plastic collapse mechanism

Figure 6: Simple frame: equilibrium paths and collapse mechanism.

[2] D. Magisano, G. Garcea, Limit fire analysis of 3D frame structures, Engineering Structures 233 (2021) 111762. https://doi.org/https://doi.org/10.1016/j.engstruct.2020.111762.

[3] D. Magisano, G. Garcea, Fiber-based shakedown analysis of three-dimensional frames under multiple load combinations: Mixed finite elements and incremental-iterative solution, International Journal for Numerical Methods in Engineering 121 (17) (2020) 3743–3767. https://doi.org/10.1002/nme.6380

[4] M. Petrangeli, P. E. Pinto, V. Ciampi, Fiber Element for Cyclic Bending and Shear of RC Structures. I: Theory, Journal of Engineering Mechanics 125 (9) (1999) 994–1001. https://doi.org/10.1061/(ASCE)0733-9399(1999)125:9(994)

[5] A. Marini, E. Spacone, Analysis of reinforced concrete elements including shear effects, ACI Structural Journal 103 (5) (2006) 645–655. https://doi.org/10.14359/16916.

[6] A. Saritas, F. C. Filippou, Inelastic axial-flexure-shear coupling in a mixed formulation beam finite element, International Journal of Non-Linear Mechanics 44 (8) (2009) 913–922. https://doi.org/https://doi.org/10.1016/j.ijnonlinmec.2009.06.007.

[7] J. Navarro Gregori, P. Miguel Sosa, M. Fernández Prada, F. C. Filippou, A 3D numerical model for reinforced and prestressed concrete elements subjected to combined axial, bending, shear and torsion loading, Engineering Structures 29 (12) (2007) 3404–3419. https://doi.org/https://doi.org/10.1016/j.engstruct.2007.09.001

[8] A. Papachristidis, M. Fragiadakis, M. Papadrakakis, A 3d fibre beam-column element with shear modelling for the inelastic analysis of steel structures, Computational Mechanics 45 (6) (2010) 553–572. https://doi.org/10.1007/s00466-010-0470-8

[9] F. Gruttmann, R. Sauer, W. Wagner, Theory and numerics of three-dimensional beams with elastoplastic material behaviour, International Journal for Numerical Methods in Engineering 48 (12) (2000) 1675–1702. https://doi.org/https://doi.org/10.1002/1097-0207(20000830)48:12<1675::AID-NME957>3.0.CO;2-6.

[10] J.-M. Battini, C. Pacoste, Plastic instability of beam structures using co-rotational elements, Computer Methods in Applied Mechanics and Engineering 191 (51) (2002) 5811–5831. https://doi.org/https://doi.org/10.1016/S0045-7825(02)00498-X.

[11] J. Bleyer, P. de Buhan, A numerical approach to the yield strength of shell structures, European Journal of Mechanics - A/Solids 59 (2016) 178–194. https://doi.org/https://doi.org/10.1016/j.euromechsol.2016.03.002

[12] R. L. Taylor, F. C. Filippou, A. Saritas, F. Auricchio, A mixed finite element method for beam and frame problems, Computational Mechanics 31 (1) (2003) 192–203. https://doi.org/10.1007/s00466-003-0410-y

[13] D. Magisano, F. Liguori, L. Leonetti, G. Garcea, Minkowski plasticity in 3d frames: Decoupled construction of the cross-section yield surface and efficient stress update strategy, International Journal for Numerical Methods in Engineering 116 (7) (2018) 435–464. https://doi.org/10.1002/nme.5931

[14] N. A. Nodargi, P. Bisegna, A mixed finite element for the nonlinear analysis of in-plane loaded masonry walls, International Journal for Numerical Methods in Engineering 120 (11) (2019) 1227–1248. https://doi.org/https://doi.org/10.1002/nme.6179.

[15] D. Magisano, A. Corrado, New robust and efficient global iterations for large deformation finite element analysis of beams and shells with material nonlinearity, Computer Methods in Applied Mechanics and Engineering 406 (2023) 115900. https://doi.org/https://doi.org/10.1016/j.cma.2023.115900.

[16] A. Genoese, A. Genoese, A. Bilotta, G. Garcea, A generalized model for heterogeneous and anisotropic beams including section distortions, Thin-Walled Structures 74 (2014) 85–103. https://doi.org/https://doi.org/10.1016/j.tws.2013.09.019

[17] D. Magisano, G. Garcea, A 3D distributed plasticity beam-column element for metal structures considering tangential stresses and warping with minimal dofs, Thin-Walled Structures 196 (2024) 111463. https://doi.org/https://doi.org/10.1016/j.tws.2023.111463

[18] F. S. Liguori, A. Madeo, G. Garcea, A dual decomposition of the closest point projection in incremental elasto-plasticity using a mixed shell finite element, International Journal for Numerical Methods in Engineering 123 (24) (2022) 6243–6266. http://arxiv.org/abs/https://onlinelibrary.wiley.com/doi/pdf/10.1002/nme.7112